Charge effect on hindrance factors for diffusion and convection of solute in pores II

Takeshi Akinaga‡, Hideyuki O-tani and Masako Sugihara-Seki

Department of Pure and Applied Physics, Kansai University, Yamate-cho, Suita, Osaka, 564-8680, JAPAN

E-mail: r091077@kansai-u.ac.jp

Abstract. Diffusion and convection of solute suspended in a fluid across porous membranes are known to be reduced compared in bulk solution, due to the fluid mechanical interaction between the solute and the pore wall as well as steric restriction. If the solute and the pore wall are electrically charged, the electrostatic interaction between them could affect the hindrance to diffusion and convection. In the present study, the transport of charged spherical solutes through charged circular cylindrical pores filled with an electrolyte solution containing small ions was studied numerically, by using a fluid mechanical and electrostatic model. Based on a mean field theory, the electrostatic interaction energy between the solute and the pore wall was estimated from the Poisson-Boltzmann equation, and the charge effect on the solute transport was examined for the solute and pore wall of like charge. The results were compared with those obtained from the linearized form of the Poisson-Boltzmann equation, i.e. the Debye-Hückel equation.

Keywords: Electrical Charge Effect, Poisson-Boltzmann equation, Partition coefficient, Hindrance factors

‡ Corresponding author: r091077@kansai-u.ac.jp

1. Introduction

Material transport across porous membranes is encountered in a wide variety of biological and engineering fields. In such transport phenomena, charge of porous membranes or solutes frequently plays an important role in regulating the material exchange. For example, it was shown that for similar size globular proteins, ribonuclease and α-lactalbumin, the permeability of mesenteric microvessels to positively charged ribonuclease was twice that to negatively charged α-lactalbumin (Adamson et al. 1988). Together with experimental studies, theoretical analyses have been also performed for long time about the electrostatic interaction between charged solute and pore wall and its effect on transport phenomena (Curry 1984, Probstein 2003, Truskey et al. 2004).

Smith & Deen (1980, 1983) developed a model of electrostatic double-layer interaction between a spherical solute and a circular cylindrical pore to estimate equilibrium partitioning of solutes between pore and bulk solution, when the solute and pore wall are charged. Based on a continuum, point-charge description of the double layer, the electric field around a solute in an electrolyte solution can be described by the so-called Poisson-Boltzmann (PB) equation. They simplified the problem by adopting a linearized form of the PB equation, i.e. the Debye-Hückel (DH) equation to calculate the electrical potential. Evidently from the derivation, this approximation is appropriate under the condition of $|F\psi/RT| \ll 1$ (see equations (20) and (21)), where ψ is the electrical potential, F is the Faraday constant, R is the gas constant, and T is the absolute temperature. For the same configuration with Smith & Deen (1980, 1983), i.e., a charged spherical solute in a charged circular cylindrical pore, a recent study of Bhalla & Deen (2009) reported that the values of the Boltzmann factor $\exp(-E/kT)$, which is a main factor determining the solute partitioning as well as the diffusion and convection of solutes, are nearly identical, irrespective of whether they are derived from the PB equation or from the DH equation, even for maximum values of $|F\psi/RT|$ exceeding unity, where k is the Boltzmann constant and E is the interaction energy between the solute and the pore including steric and electrostatic interactions. Thus, they concluded that the DH equation provides sufficiently accurate results for the interaction energy E in calculating transport coefficients such as the osmotic reflection coefficient.

In a previous study, we used the DH equation to analyze the transport of a charged spherical solute across porous membranes with charged circular cylindrical pores filled with an electrolyte solution (O-tani et al. 2011). Assuming that the radius of the pore and that of the solute molecule greatly exceed that of the solvent, we carried out fluid mechanical analyses to calculate the flow field around a solute in the pore to estimate the drag coefficients on the solute. We computed the electrical potential around the solute in the electrolyte solution based on a mean field theory to provide the interaction energy between the solute and pore of like charge. Combining the results of the fluid mechanical and electrostatic analyses, we estimated the rate of the diffusive and convective transport of solute across the pore (O-tani et al. 2011). However, our recent preliminary study suggested that the values of the Boltzmann factor estimated from the nonlinear PB and

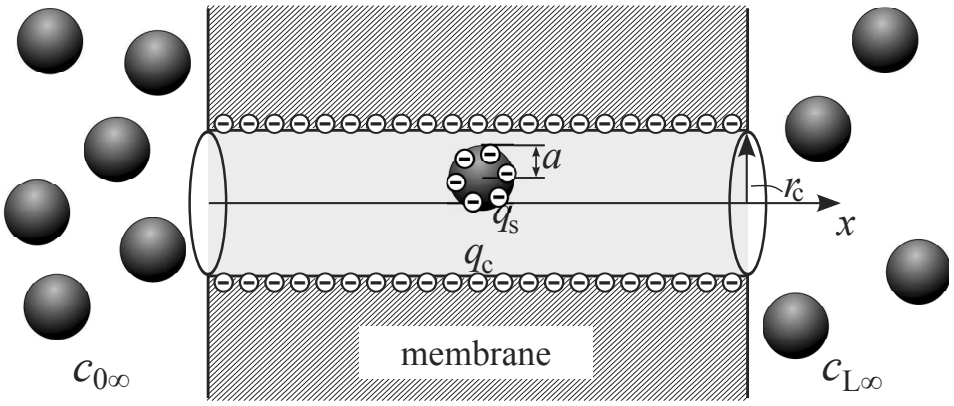

Figure 1. Sketch of the solute transport across a membrane with circular cylindrical pores of radius r_c and length L. Spherical solutes of radius a are suspended in an electrolyte solution containing small cations and anions. The surfaces of the pore wall and solutes are electrically charged with densities q_c and q_s, respectively. The membrane is placed between two solutions of solute concentration $c_{0\infty}$ and $c_{L\infty}$. The ion concentrations are the same on both sides of the membrane.

linear DH formulations are not always comparable, and the difference between them may become rather significant, especially in the cases of large charge densities and/or low ion concentrations (Akinaga & Sugihara-Seki 2011).

In the present study, therefore, we recalculate the electrical potential based on the PB equation, instead of the DH equation, for a charged spherical solute in a charged cylindrical pore, and compare the Boltzmann factor obtained from the PB equation and from the DH equation. The effect of solute and pore charge on the rate of the diffusive and convective transport of solute across cylindrical pores is examined in the framework of a nonlinear formulation.

2. Formulation and methods

The model to describe the solute transport across porous membranes is the same with O-tani et al. (2011). Briefly, we consider diffusive and convective transport of spherical solute of radius a across a porous membrane with circular cylindrical pores of radius r_c and length L ($r_c \ll L$), as shown in figure 1. The membrane is placed between two solutions differing in solute concentration, $c_{0\infty}$ and $c_{L\infty}$ ($c_{0\infty} > c_{L\infty}$). The radii of the solute and the pore are assumed to be much larger than that of the solvent molecules, so that the solute is treated as a particle and the solvent as a continuum. The solute and the pore wall have uniform constant surface charge of density q_s and q_c, respectively, and the solvent is an electrolyte solution containing small cations and anions. The ions are so small compared to the solute or the pore that a point-charge description of the electric double layer is employed, and the electrolyte solution is regarded as a Newtonian fluid with viscosity μ. For simplicity, we restrict the analysis to the cases of dilute solutions, solute and pore surfaces of like charge, and univalent-univalent electrolytes. The bulk

electrolyte concentrations on both sides of the membrane are assumed to be equal, say C_0.

Taking the x-axis along the centerline of the pore, we assume mechanical and thermal equilibrium in the x-direction such that the fluid mechanical force exerted on a solute is balanced with the gradient of the chemical potential of the solute. This condition yields for a solute translating with velocity U in the x-direction, immersed in a mean flow V,

$$kT\frac{1}{c}\frac{\partial c}{\partial x} = -6\pi\mu a\left(-UF_{\mathrm{t}} + VF_0\right) \tag{1}$$

where c is the solute concentration, F_{t} and F_0 represent the drag coefficients defined as $F_{\mathrm{t}} = -F/6\pi\mu aU$ and $F_0 = F'/6\pi\mu aV$, where F is the hydrodynamic force exerted on the solute translating parallel to the pore axis at velocity U in an otherwise quiescent fluid, and F' is the force exerted on a stationary solute immersed in a Poiseuille flow through the pore with mean velocity V. In equation (1), the force due to solute rotation is not included, since its effect was found to be small (Sugihara-Seki 2004). We further assume an equilibrium distribution of solutes in the radial direction so that the solute concentration c is expressed as

$$c = c_0\left(x\right)\exp\left[-\frac{E\left(\beta\right) - E\left(0\right)}{kT}\right], \tag{2}$$

where $c_0(x)$ represents the solute concentration on the x-axis and $E(\beta)$ represents the solute potential when the solute center is placed at non-dimensional radial position β relative to the pore radius. Then, equation (1) leads to the expression for the axial component of the solute flux:

$$\langle N\rangle = -K_{\mathrm{d}}D_\infty\frac{d\left\langle c\right\rangle}{dx} + K_{\mathrm{c}}V\left\langle c\right\rangle \tag{3}$$

where N $(= cU)$ is the solute flux, the angle brackets indicate average over the pore cross-section, $D_\infty = kT/\left(6\pi\mu a\right)$ represents the diffusivity in an unbounded solution, and K_{d} and K_{c} are local hindrance factors for diffusion and convection, respectively, which are given by

$$K_{\mathrm{d}} = \frac{\int_0^{1-a/r_{\mathrm{c}}}\left(F_{\mathrm{t}}\left(\beta\right)\right)^{-1}\exp\left[-E\left(\beta\right)/kT\right]\beta\, d\beta}{\int_0^{1-a/r_{\mathrm{c}}}\exp\left[-E\left(\beta\right)/kT\right]\beta\, d\beta}, \tag{4}$$

$$K_{\mathrm{c}} = \frac{\int_0^{1-a/r_{\mathrm{c}}}F_0\left(\beta\right)\left(F_{\mathrm{t}}\left(\beta\right)\right)^{-1}\exp\left[-E\left(\beta\right)/kT\right]\beta\, d\beta}{\int_0^{1-a/r_{\mathrm{c}}}\exp\left[-E\left(\beta\right)/kT\right]\beta\, d\beta}. \tag{5}$$

Equation (3) can be solved to obtain

$$\langle N\rangle = K_{\mathrm{c}}V\frac{\left\langle c\right\rangle_0 - \left\langle c\right\rangle_{\mathrm{L}}e^{-Pe}}{1 - e^{-Pe}}, \tag{6}$$

where the Peclet number is defined in terms of the pore length such as

$$Pe = \frac{K_{\mathrm{c}}VL}{K_{\mathrm{d}}D_\infty}. \tag{7}$$

Here, $\langle c \rangle_0$ and $\langle c \rangle_{\mathrm{L}}$ are the averaged solute concentration at the pore entrance and exit, respectively. These quantities are related to the bulk concentrations by

$$\langle c \rangle_0 = c_{0\infty}\Phi, \tag{8}$$

$$\langle c \rangle_{\mathrm{L}} = c_{\mathrm{L}\infty}\Phi, \tag{9}$$

$$\Phi = 2\int_0^{1-a/r_{\mathrm{c}}} \exp\left[-E\left(\beta\right)/kT\right]\beta\, d\beta. \tag{10}$$

The quantity Φ defined by equation (10) is termed solute partitioning coefficient, which represents the partitioning of solute between pores and bulk solution. Substitution of equations (8) and (9) into equation (6) yields

$$\langle N \rangle = \Phi K_{\mathrm{c}} V c_{0\infty} \frac{1 - \left(c_{\mathrm{L}\infty}/c_{0\infty}\right) e^{-Pe}}{1 - e^{-Pe}}. \tag{11}$$

If we define

$$H = \Phi K_{\mathrm{d}}, \tag{12}$$

$$W = \Phi K_{\mathrm{c}}, \tag{13}$$

then equations (7) and (11) are rewritten as

$$Pe = \frac{WVL}{HD_\infty}, \tag{14}$$

$$\langle N \rangle = WVc_{0\infty} \frac{1 - \left(c_{\mathrm{L}\infty}/c_{0\infty}\right) e^{-Pe}}{1 - e^{-Pe}}. \tag{15}$$

The limiting forms of equation (15) are

$$\langle N \rangle = \frac{HD_\infty}{L}\left(c_{0\infty} - c_{\mathrm{L}\infty}\right) \quad \text{for} \quad Pe \ll 1, \tag{16}$$

$$\langle N \rangle = WVc_{0\infty} \quad \text{for} \quad Pe \gg 1. \tag{17}$$

Note that equations (16) and (17) represent the diffusive and convective transport, respectively, and H and W equal unity in the case of $a/r_{\mathrm{c}} \ll 1$ or in bulk phase. Thus, the values of H and W represent the rate of the diffusion and convection of the solute through the pore relative to the bulk phase, respectively, and are called hindrance factors.

In O-tani et al. (2011), we focused on charge effect on H and W. In the present study, we also calculate Φ as functions of the size ratio a/r_{c}, the charge densities q_{s}, q_{c}, and the ion concentration C_0. In evaluating these values from equations (10), (4), (5), (12) and (13), there are two steps before performing integrations appeared in these equations: (i) estimate of the drag coefficients F_{t} and F_0, and (ii) estimate of the interaction energy E. These procedures are the same with O-tani et al. (2011), except the use of the PB equation instead of the DH equation in step (ii).

In step (i), the Stokes equations together with the continuity equation were solved numerically to calculate the flow field around a solute placed in a pore, by employing a hp-finite element method (O-tani et al. 2011). From the velocity fields obtained for a solute translating in the x-direction in an otherwise quiescent fluid and for a stationary solute immersed in a Poiseuille flow, we computed the drag coefficients F_{t}

Table 1. Error estimation. $r_c = 10$ nm, $q_c = q_s = -0.02$ C/m^2.

order n	a/r_c	τ	Φ_{DH-N}	Φ_{PB-N}	$\frac{\Delta\Phi_{DH-N}}{\Phi^*_{DH-N}}$	$\frac{\Delta\Phi_{PB-N}}{\Phi^*_{PB-N}}$
6	0.2	3.32	4.629×10^{-4}	1.009×10^{-2}	7.714×10^{-4}	5.405×10^{-2}
7	0.2	3.32	4.626×10^{-4}	9.714×10^{-3}	1.394×10^{-4}	1.474×10^{-2}
8	0.2	3.32	4.625×10^{-4}	9.607×10^{-3}	3.947×10^{-5}	3.553×10^{-3}
9*	0.2	3.32	4.625×10^{-4}	9.573×10^{-3}	–	–
6	0.2	6.63	1.960×10^{-1}	2.586×10^{-1}	1.976×10^{-2}	1.290×10^{-1}
7	0.2	6.63	1.924×10^{-1}	2.375×10^{-1}	1.335×10^{-3}	3.686×10^{-2}
8	0.2	6.63	1.923×10^{-1}	2.312×10^{-1}	5.747×10^{-4}	9.491×10^{-3}
9*	0.2	6.63	1.922×10^{-1}	2.291×10^{-1}	–	–
6	0.2	12.84	5.707×10^{-1}	5.928×10^{-1}	1.823×10^{-1}	1.853×10^{-1}
7	0.2	12.84	5.143×10^{-1}	5.437×10^{-1}	6.553×10^{-2}	8.712×10^{-2}
8	0.2	12.84	4.912×10^{-1}	5.155×10^{-1}	1.780×10^{-2}	3.070×10^{-2}
9*	0.2	12.84	4.827×10^{-1}	5.001×10^{-1}	–	–
6	0.6	3.32	2.690×10^{-49}	9.584×10^{-21}	4.733×10^{-6}	1.072×10^{-3}
7	0.6	3.32	2.690×10^{-49}	9.576×10^{-21}	2.254×10^{-8}	1.891×10^{-4}
8	0.6	3.32	2.690×10^{-49}	9.574×10^{-21}	3.544×10^{-8}	3.003×10^{-5}
9*	0.6	3.32	2.690×10^{-49}	9.574×10^{-21}	–	–
6	0.6	6.63	3.992×10^{-7}	8.427×10^{-6}	7.642×10^{-5}	2.610×10^{-3}
7	0.6	6.63	3.991×10^{-7}	8.409×10^{-6}	3.875×10^{-6}	4.972×10^{-4}
8	0.6	6.63	3.991×10^{-7}	8.405×10^{-6}	4.031×10^{-7}	8.433×10^{-5}
9*	0.6	6.63	3.991×10^{-7}	8.405×10^{-6}	–	–
6	0.6	12.84	2.882×10^{-2}	3.217×10^{-2}	8.172×10^{-3}	2.083×10^{-2}
7	0.6	12.84	2.861×10^{-2}	3.166×10^{-2}	7.548×10^{-4}	4.720×10^{-3}
8	0.6	12.84	2.859×10^{-2}	3.154×10^{-2}	1.054×10^{-4}	1.005×10^{-3}
9*	0.6	12.84	2.858×10^{-2}	3.151×10^{-2}	–	–

and F_0 as functions of the radial position of the solute center β and the size ratio a/r_c. As noted in O-tani et al. (2011), although our estimates of the drag coefficients suggested considerable difference from existing studies, depending on the radial position and the size ratio, this difference was found to have a minor effect on the hindrance factors. In the present study, we adopt the values of F_t and F_0 from O-tani et al. (2011).

In step (ii), the Gauss's law is expressed in terms of the electrical potential ψ and the concentrations of monovalent cation and anion C_+ and C_- as

$$\nabla^2\psi = -\frac{F}{\varepsilon}\left(C_+ - C_-\right), \tag{18}$$

where ε is the solvent dielectric permittivity. Assuming the Boltzmann distribution of ions such as

$$C_\pm = C_0 \exp\left(\mp F\psi/FT\right), \tag{19}$$

we obtain the PB equation

$$\nabla^2\psi = \frac{2FC_0}{\varepsilon}\sinh\left(F\psi/RT\right). \tag{20}$$

If $|F\psi/FT| \ll 1$, then equation (20) can be reduced to the so-called Debye-Hückel equation:

$$\nabla^2\psi = \frac{1}{\lambda_{\mathrm{D}}^2}\psi, \tag{21}$$

where $\lambda_{\mathrm{D}} = \left[\varepsilon RT/2F^2C_0\right]^{1/2}$ is the Debye length, defined for a univalent-univalent electrolyte.

Equation (20) was solved numerically by a spectral element method, subject to the boundary condition corresponding to the prescribed surface charge densities. The method of numerical computations and error assessments are described in Akinaga et al. (2008).

Similarly to our previous error estimation for the potential energy (Akinaga et al. (2008)), we examined how the obtained values of the partition coefficient vary with changing the truncation order n of the interpolation functions in the spectral element method. The 6th and 7th columns in Table 1 show the relative errors of the partition coefficient compared to the value of $n = 9$ at $q_{\mathrm{s}} = q_{\mathrm{c}} = -0.02$ C/m^2. It is seen from Table 1 that the relative error decreases with increasing the truncation order n for constant a/r_{c} and τ. Table 1 shows that the relative error of the partition coefficient at $n = 8$ is at most about 3 percent in the case of high charge density. In the case of low charge density ($q_{\mathrm{s}} = q_{\mathrm{c}} = -0.005$ C/m^2), the relative errors are much smaller than the corresponding values shown in Table 1. Thus, we adopted $n = 8$ in the current study. The detailed procedures in steps (i) and (ii) are described in O-tani et al. (2011).

In the following section, we shall make a comparison to the results obtained from the PB equation (equation (20)) and from the DH equation (equation (21)). We denote the former as PB-N and the latter as DH-N. As may be evident from equations (10), (4) and (5), the Boltzmann exponential factor $\exp\left[-E\left(\beta\right)/kT\right]$ plays a key role in determining the values of Φ, H and W. The Boltzmann factor reflects the relative probability of finding a solute at a given radial position β in the pore. Thus, beginning with the Boltzmann factor, we consider the solute partitioning coefficient Φ, the hindrance factors H and W.

Smith & Deen (1980, 1983) solved the DH equation by an analytical method combining general solutions expressed in cylindrical and spherical coordinates to calculate the partitioning coefficient. They approximated their analytical solution by truncating series expansions. The details of their method were elaborated in Smith (1981) and summarized in the appendix of Bhalla & Deen (2009). By adopting their method, we also calculated the approximate solution of the DH equation, and denote the results as DH-A.

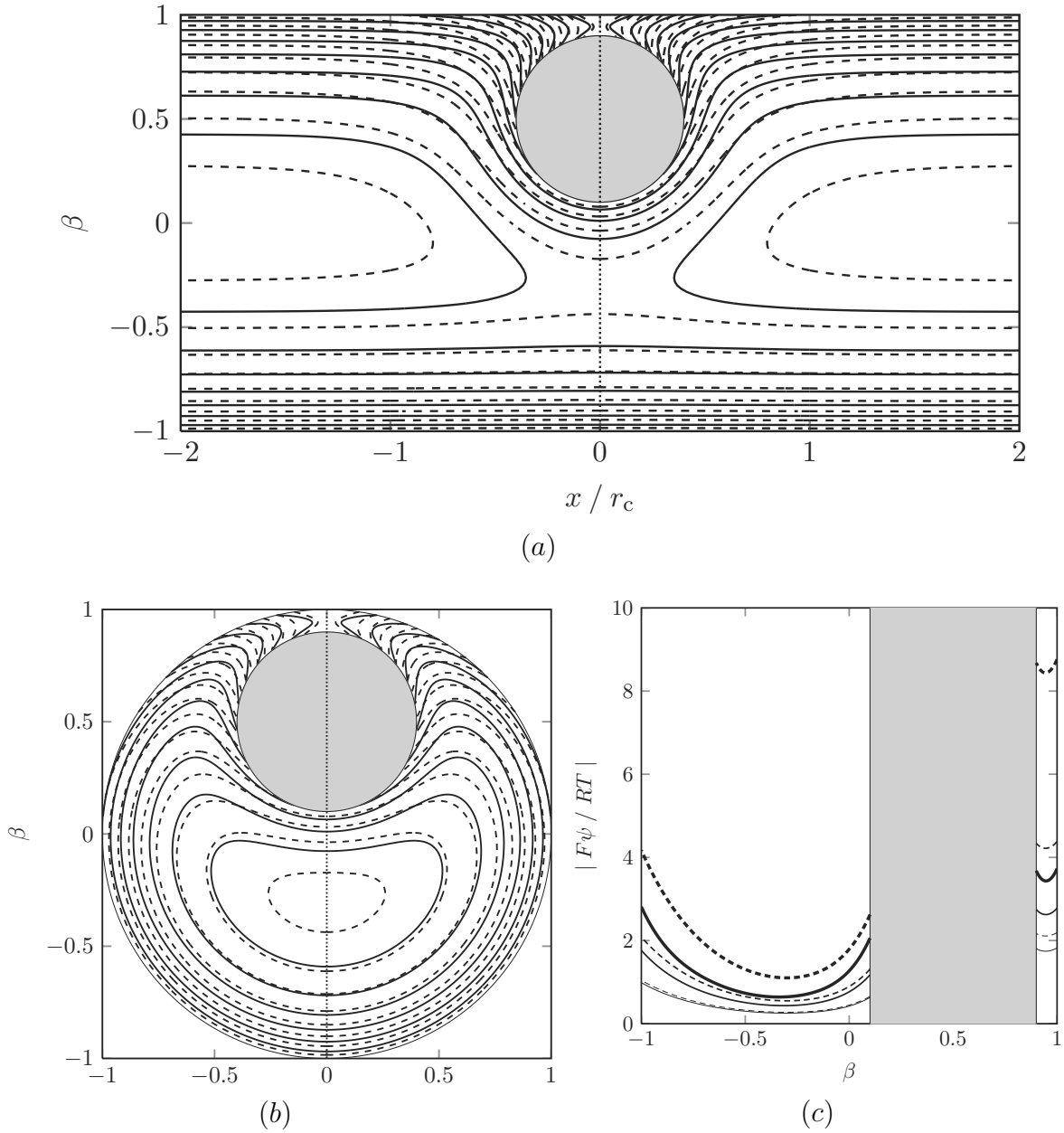

Figure 2. (a) The contours of electrical potential in a longitudinal section of the pore containing the centerline of the pore and the center of a solute, (b) the contours of electrical potential in the cross-section of the pore containing the solute center, and (c) profiles of the electrical potential along the dotted line in figures 2(a) and (b). The parameter values are $r_c = 10$ nm, $a = 4$ nm, $q_s = q_c = -0.01$ C/m^2, $C_0 = 0.01$ M, and the solute center is placed at $\beta = 0.5$. The solid lines represent the results of PB-N, and the dashed lines represent the results of DH-N. The thin and thick lines in figure 2(c) are the corresponding profiles for $q_s = q_c = -0.005$ and -0.02 C/m^2, respectively, with the other parameters unchanged. In figures (a) and (b), the interval between neighboring contours is $F\Delta\psi/RT = 0.2$.

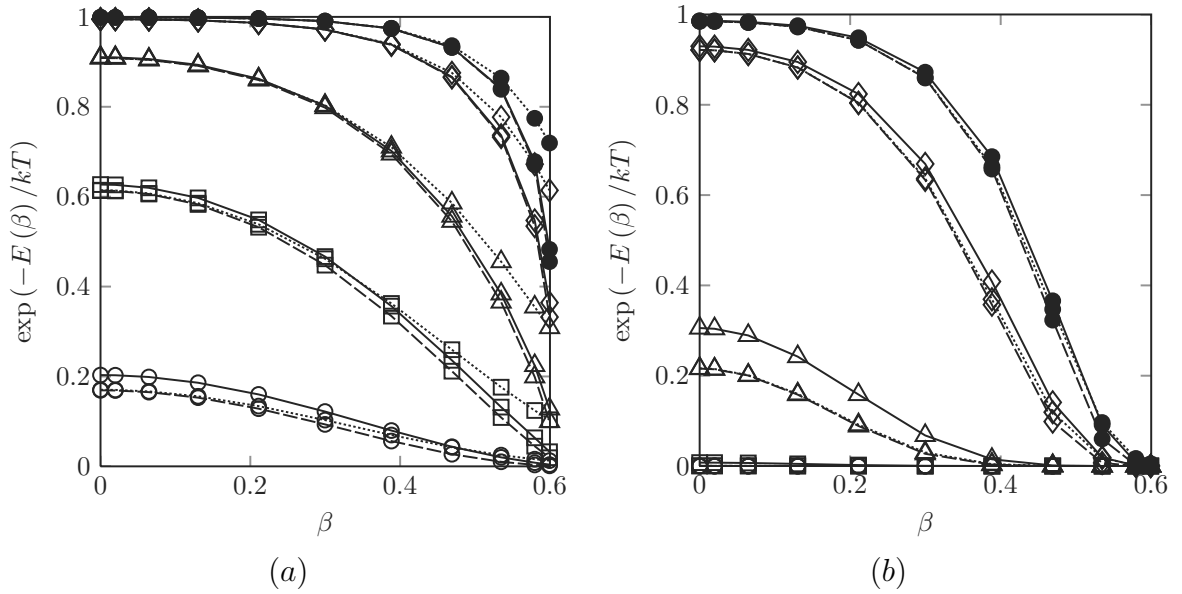

Figure 3. Boltzmann factor $\exp[-E(\beta)/kT]$ as a function of the relative radial position of the solute center for $r_c = 10$ nm, $a = 4$ nm, at (a) $q_s = q_c = -0.005$ C/m^2 and at (b) $q_s = q_c = -0.02$ C/m^2. The ion concentrations are $C_0 = 0.01$ M (open circles), 0.02 M (squares), 0.04 M (triangles), 0.1 M (diamonds), and 0.15 M (closed circles), corresponding to $\tau = 3.32$, 4.69, 6.63, 10.49 and 12.84, respectively, for aqueous solutions at $T = 310$ K. The solid lines represent the results of PB-N, the dashed lines represent the results of DH-N, and the dotted lines represent the results of DH-A.

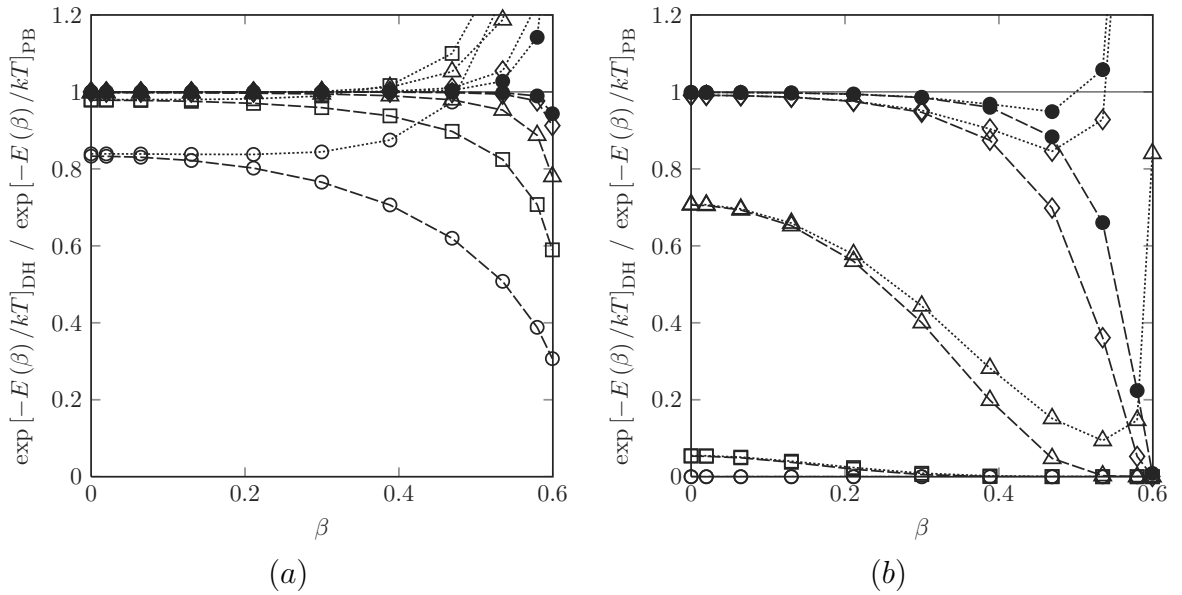

Figure 4. Ratios of the Boltzmann factors obtained from the DH equation and the corresponding values obtained from the PB equation, $\exp[-E(\beta)/kT]_{\mathrm{DH-N}}$ / $\exp[-E(\beta)/kT]_{\mathrm{PB-N}}$ (dashed lines) and $\exp[-E(\beta)/kT]_{\mathrm{DH-A}}$ / $\exp[-E(\beta)/kT]_{\mathrm{PB-N}}$ (dotted lines), for $r_c = 10$ nm, $a = 4$ nm, at (*a*) $q_s = q_c = -0.005$ C/m^2 and at (*b*) $q_s = q_c = -0.02$ C/m^2. The ion concentrations are $C_0 = 0.01$ M (open circles), 0.02 M (squares), 0.04 M (triangles), 0.1 M (diamonds), and 0.15 M (closed circles), corresponding to $\tau = 3.32$, 4.69, 6.63, 10.49 and 12.84, respectively, for aqueous solutions at $T = 310$ K.

3. Results

Figures 2(a) and 2(b) show the contours of the electrical potential for $r_c = 10$ nm, $a = 4$ nm, $q_s = q_c = -0.01$ C/m^2 and $C_0 = 0.01$ M, with the solute center placed at $\beta = 0.5$ from the pore centerline. Profiles of the electrical potential along the dotted line in figures 2(a) and (b) are plotted in figure 2(c). The corresponding profiles for $q_s = q_c = -0.005$ C/m^2 and $q_s = q_c = -0.02$ C/m^2 with the other parameter unchanged are also plotted by thin lines and thick lines, respectively, in figure 2(c). In each figure, the solid lines represent the results of PB-N, and the dashed lines represent the results of DH-N. A strong interaction of the electric double layer formed around the solute and that near the pore wall is seen in figures 2(a) and 2(b). Figures 2(a)-(c) indicate that the magnitudes of the electrical potential obtained from the DH equation are larger than the corresponding values from the PB equation, and the differences between them are significant in the gap region between the solute and the pore wall. Figure 2(c) shows that this difference becomes larger as the magnitude of the charge density is increased. It can be also shown that the difference is increased with decreasing ion concentration C_0 (not shown).

The Boltzmann factor $\exp[-E(\beta)/kT]$ is plotted as a function of the radial position of the solute center for $r_c = 10$ nm, $a = 4$ nm and $C_0 = 0.01$, 0.02, 0.04, 0.10 and 0.15 M, at $q_s = q_c = -0.005$ C/m^2 in figure 3(a) and at $q_s = q_c = -0.02$ C/m^2 in figure 3(b). If we define a non-dimensional parameter $\tau = r_c/\lambda_D$, the cases of $C_0 = 0.01$, 0.02, 0.04, 0.10 and 0.15 M correspond to $\tau = 3.32$, 4.69, 6.63, 10.49 and 12.84, respectively, for aqueous solutions at $T = 310$ K. In figures 3(a) and (b), the solid lines represent the results of PB-N, the dashed lines represent the results of DH-N, and the dotted lines represent the results of DH-A. Figures 3(a) and (b) show a decrease in Boltzmann factor as the radial position β is increased from 0 to $1-a/r_c$ ($= 0.6$) for given τ or τ is deceased for given β. The former trend indicates that the solute is more likely to be placed closer to the pore centerline, due to the electrostatic repulsive interaction between the solute and pore charge. The latter trend is because a decrease in τ or an increase in Debye length strengthens the electrostatic interaction, which results in stronger exclusion of solutes from the pore.

It is seen from figures 3(a) and (b) that the results of DH-A and DH-N, $\exp[-E(\beta)/kT]_{\mathrm{DH-A}}$ and $\exp[-E(\beta)/kT]_{\mathrm{DH-N}}$, show a good agreement except for the solute placed close to the pore wall, i.e. $\beta \sim 1 - a/r_c$, and the values of $\exp\left[-E\left(\beta\right)/kT\right]_{\mathrm{DH-A}}$ are always larger than the corresponding values of $\exp\left[-E\left(\beta\right)/kT\right]_{\mathrm{DH-N}}$. As β is increased up to $1 - a/r_c$ ($= 0.6$), the difference between them is more evident in figure 3(a). Although this discrepancy near $\beta \sim 1 - a/r_c$ is invisible in figure 3(b), there is a large relative difference between them in this case as well, which will be seen in figure 4.

In order to show the difference of the Boltzmann factors obtained from the PB equation, $\exp\left[-E\left(\beta\right)/kT\right]_{\mathrm{PB-N}}$, and the corresponding values obtained from the DH equation, $\exp[-E(\beta)/kT]_{\mathrm{DH-N}}$ and $\exp\left[-E\left(\beta\right)/kT\right]_{\mathrm{DH-A}}$, we plotted the

ratios of $\exp\left[-E\left(\beta\right)/kT\right]_{\mathrm{DH-N}}$ / $\exp\left[-E\left(\beta\right)/kT\right]_{\mathrm{PB-N}}$ and $\exp\left[-E\left(\beta\right)/kT\right]_{\mathrm{DH-A}}$ / $\exp\left[-E\left(\beta\right)/kT\right]_{\mathrm{PB-N}}$ in figure 4, for $r_{\mathrm{c}} = 10$ nm, $a = 4$ nm and $\tau = 3.32$, 4.69, 6.63, 10.49 and 12.84 at $q_{\mathrm{s}} = q_{\mathrm{c}} = -0.005$ and -0.02 C/m^2. Figures 4(a) and (b) show that the ratio of $\exp\left[-E\left(\beta\right)/kT\right]_{\mathrm{DH-N}}$ / $\exp\left[-E\left(\beta\right)/kT\right]_{\mathrm{PB-N}}$ is always smaller than unity, reflecting the fact that the interaction energy $E(\beta)$ is overestimated based on the DH equation. It is also seen that the ratio of $\exp\left[-E\left(\beta\right)/kT\right]_{\mathrm{DH-N}}$ / $\exp\left[-E\left(\beta\right)/kT\right]_{\mathrm{PB-N}}$ decreases monotonically with increasing β from 0 to $1-a/r_{\mathrm{c}}$ or with decreasing τ. This may be understood from figure 2, which shows large difference in electrical potentials of PB-N and DH-N in the gap region between the solute and the pore wall. This difference is more enhanced for larger β and smaller τ.

In the case of low charge density ($q_{\mathrm{s}} = q_{\mathrm{c}} = -0.005$ C/m^2), figure 4(a) shows that the ratio of $\exp\left[-E\left(\beta\right)/kT\right]_{\mathrm{DH-N}}$ / $\exp\left[-E\left(\beta\right)/kT\right]_{\mathrm{PB-N}}$ remains close to unity for large τ ($\geq$ 4.69) over almost the whole range of β except for $\beta \sim 1 - a/r_{\mathrm{c}}$, while in the case of high charge density ($q_{\mathrm{s}} = q_{\mathrm{c}} = -0.02$ C/m^2), figure 4(b) shows that the ratio is much smaller than unity for small τ (≤ 6.63) even for the solute placed near the pore centerline. It is interesting to note that the ratio of $\exp[-E(\beta)/kT]_{\mathrm{DH-N}}$ / $\exp[-E(\beta)/kT]_{\mathrm{PB-N}}$ is as low as about 0.05 for $\tau = 4.69$ and it is nearly 0 for τ= 3.32 in figure 4(b), whereas the Boltzmann factors themselves are visually indistinguishable in both cases, given the linear scale in figure 3(b). This is because the interaction energy $E(\beta)/kT$ is so large in those cases that the Boltzmann factor $\exp[-E(\beta)/kT]$ is extremely small.

With regard to DH-A, figure 4(a) shows that an increase in β increases the ratio of $\exp[-E(\beta)/kT]_{\mathrm{DH-A}}$ / $\exp[-E(\beta)/kT]_{\mathrm{PB-N}}$ beyond unity, and the ratio rises rapidly with β approaching $(1 - a/r_{\mathrm{c}})$. The rapid rise of $\exp[-E(\beta)/kT]_{\mathrm{DH-A}}$ / $\exp[-E(\beta)/kT]_{\mathrm{PB-N}}$ near $\beta \sim (1 - a/r_{\mathrm{c}})$ is also seen in figure 4(b), indicating that the DH-A underestimates the interaction energy for large β.

Multiplying the Boltzmann factor by β and integrating it over the pore cross-section yields the solute partitioning coefficient Φ (equation (10)). As evident from equations (8) and (9), the quantity Φ represents the ratio of the solute concentration at the pore ends relative to the bulk solution. Figure 5 shows Φ as a function of τ, for $r_{\mathrm{c}} = 10$ nm, $a = 2$, 4, 6 nm, $q_{\mathrm{s}} = q_{\mathrm{c}} = -0.005$ and -0.02 C/m^2. For small τ, electrostatic effects are so large that solutes are excluded from the pores, while for large τ, electrostatic effects are unimportant. Thus, each curve increases monotonically with increasing τ and approaches an asymptotic limit corresponding to purely steric exclusion, $(1-a/r_{\mathrm{c}})^2$. This limiting value can be easily obtained from equation (10) for $E(\beta) = 0$ at $0 \leq \beta \leq (1 - a/r_{\mathrm{c}})$.

In general, the difference of Φ values between linear and nonlinear formulations is large for small τ, while it is small for large τ. In the case of low charge density ($q_{\mathrm{s}} = q_{\mathrm{c}} = -0.005$ C/m^2), open symbols in figures 5(a) and (b) show that the $\Phi_{\mathrm{DH-N}}$ values are comparable to those of $\Phi_{\mathrm{PB-N}}$ and the difference between them becomes noticeable only for small τ. In contrast, the difference between the $\Phi_{\mathrm{DH-A}}$ values and the $\Phi_{\mathrm{PB-N}}$ values is evident at low charge density, resulting from that the Boltzmann

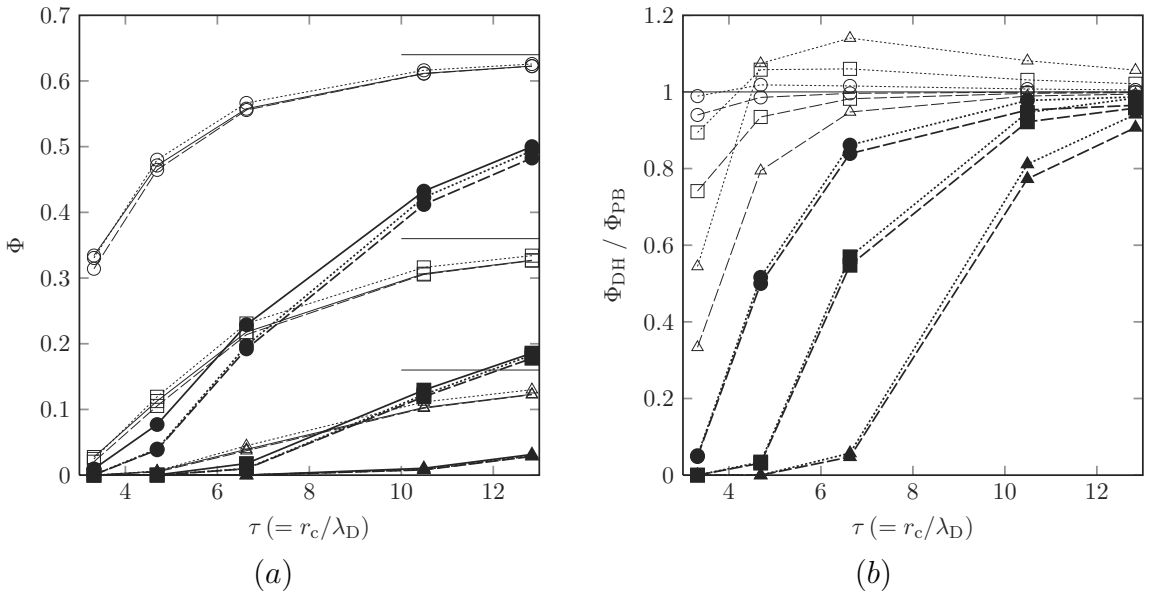

Figure 5. (a) Partitioning coefficients $\Phi_{\mathrm{PB-N}}$ (solid lines), $\Phi_{\mathrm{DH-N}}$ (dashed lines) and $\Phi_{\mathrm{DH-A}}$ (dotted lines) for $r_{\mathrm{c}} = 10$ nm, $q_{\mathrm{s}} = q_{\mathrm{c}} = -0.005$, -0.02 C/m^2, and (b) ratios of partitioning coefficients obtained from the DH equation and the corresponding values obtained from the PB equation, $\Phi_{\mathrm{DH-N}}$ / $\Phi_{\mathrm{PB-N}}$ (dashed lines) and $\Phi_{\mathrm{DH-A}}$ / $\Phi_{\mathrm{PB-N}}$ (dotted lines). The size ratios are $a/r_{\mathrm{c}} = 0.2$ (circles), 0.4 (squares), and 0.6 (triangles). Open symbols represent the case of $q_{\mathrm{s}} = q_{\mathrm{c}} = -0.005$ C/m^2 and closed symbols represent the case of $q_{\mathrm{s}} = q_{\mathrm{c}} = -0.02$ C/m^2.

factors of DH-A are larger than those of PB-N or DH-N for the solute placed near the pore wall ($\beta \sim 1 - a/r_{\mathrm{c}}$), as shown in figures 3(a) and 4(a). Figure 5(b) shows that, as τ is increased for given a/r_{c}, the ratio $\Phi_{\mathrm{DH-A}}$ / $\Phi_{\mathrm{PB-N}}$ increases from below unity and reaches a maximum at a certain β, beyond which the ratio decreases to approach unity. This behavior is different from the monotonic increase in $\Phi_{\mathrm{DH-N}}$ / $\Phi_{\mathrm{PB-N}}$ with increasing τ. At large charge density ($q_{\mathrm{s}} = q_{\mathrm{c}} = -0.02$ C/m^2), closed symbols in figure 5(b) show that an increase in τ increases both ratios of $\Phi_{\mathrm{DH-N}}$ / $\Phi_{\mathrm{PB-N}}$ and $\Phi_{\mathrm{DH-A}}$ / $\Phi_{\mathrm{PB-N}}$ monotonically from nearly zero to unity.

By using equations (12) and (13), the hindrance factors H and W were computed, and the obtained results of H and W are plotted in figures 6 and 7 as functions of τ, for $r_{\mathrm{c}} = 10$ nm, $a = 2$, 4, 6 nm, and $q_{\mathrm{s}} = q_{\mathrm{c}} = -0.005$ and -0.02 C/m^2. In the calculation, we adopted the values of F_{t} and F_0 of O-tani et al. (2011). Similarly to the behavior of the partitioning coefficient shown in figure 5, the hindrance factors H and W increase with increasing τ for given a/r_{c} or decreasing charge densities q_{s}, q_{c} for given τ. Their differences between linear and nonlinear formulations also show similar dependence on τ and charge densities q_{s}, q_{c} with the partitioning coefficient Φ. In short, the DH-N values of H and W provide good approximation to the PB-N values at low charge densities and large τ, and an increase in charge densities or a decrease in τ makes the DH-N values smaller compared to the PB-N values. On the other hand, the DH-A values of H and W are higher than the PB-N values at low charge density ($q_{\mathrm{s}} = q_{\mathrm{c}} = -0.005$ C/m^2) except

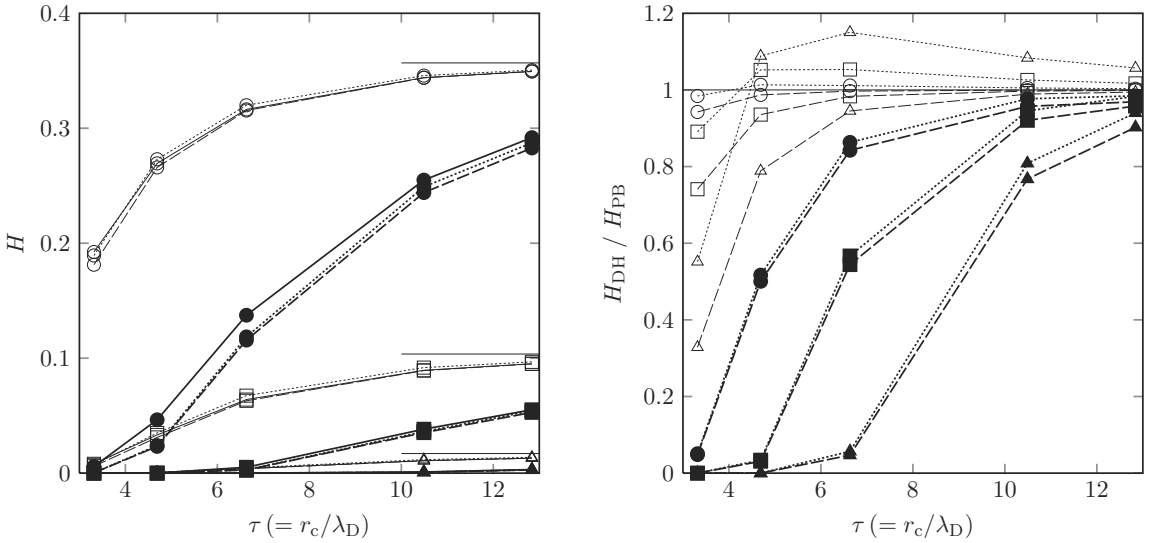

Figure 6. (a) Hindrance factors $H_{\mathrm{PB-N}}$ (solid lines), $H_{\mathrm{DH-N}}$ (dashed lines) and $H_{\mathrm{DH-A}}$ (dotted lines) for $r_{\mathrm{c}} = 10$ nm, $q_{\mathrm{s}} = q_{\mathrm{c}} = -0.005$, -0.02 C/m^2, and (b) ratios of hindrance factors obtained from the DH equation and the corresponding values obtained from the PB equation, $H_{\mathrm{DH-N}}$ / $H_{\mathrm{PB-N}}$ (dashed lines) and $H_{\mathrm{DH-A}}$ / $H_{\mathrm{PB-N}}$ (dotted lines). The size ratios are $a/r_{\mathrm{c}} = 0.2$ (circles), 0.4 (squares), and 0.6 (triangles). Open symbols represent the case of $q_{\mathrm{s}} = q_{\mathrm{c}} = -0.005$ C/m^2 and closed symbols represent the case of $q_{\mathrm{s}} = q_{\mathrm{c}} = -0.02$ C/m^2.

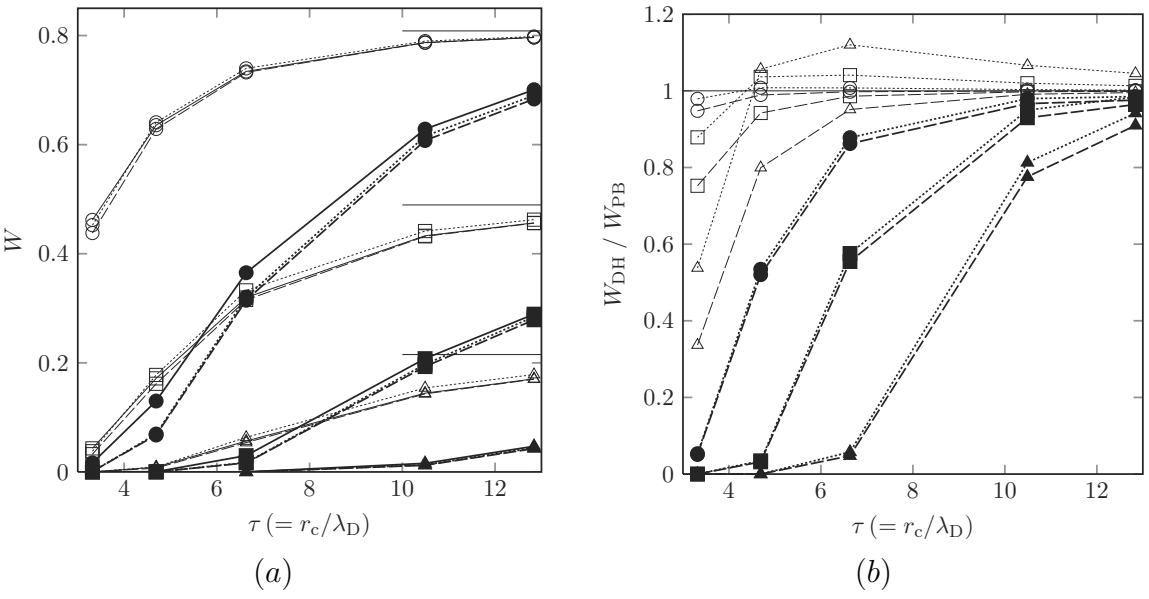

Figure 7. (a) Hindrance factors $W_{\mathrm{PB-N}}$ (solid lines), $W_{\mathrm{DH-N}}$ (dashed lines) and $W_{\mathrm{DH-A}}$ (dotted lines) for $r_{\mathrm{c}} = 10$ nm, $q_{\mathrm{s}} = q_{\mathrm{c}} = -0.005$, -0.02 C/m^2, and (b) ratios of hindrance factors obtained from the DH equation and the corresponding values obtained from the PB equation, $W_{\mathrm{DH-N}}$ / $W_{\mathrm{PB-N}}$ (dashed lines) and $W_{\mathrm{DH-A}}$ / $W_{\mathrm{PB-N}}$ (dotted lines). The size ratios are $a/r_{\mathrm{c}} = 0.2$ (circles), 0.4 (squares), and 0.6 (triangles). Open symbols represent the case of $q_{\mathrm{s}} = q_{\mathrm{c}} = -0.005$ C/m^2 and closed symbols represent the case of $q_{\mathrm{s}} = q_{\mathrm{c}} = -0.02$ C/m^2.

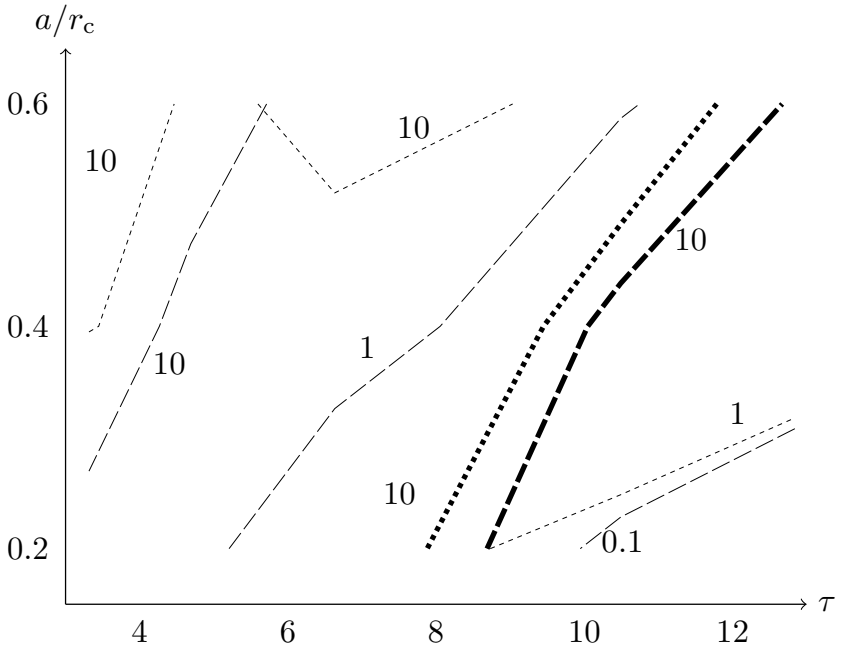

Figure 8. The relative difference of the partition coefficient $\Delta\Phi/\Phi_{\mathrm{PB-N}}$, where $\Delta\Phi$ represents either $|\Phi_{\mathrm{PB-N}} - \Phi_{\mathrm{DH-A}}|$ (dotted lines) or $|\Phi_{\mathrm{PB-N}} - \Phi_{\mathrm{DH-N}}|$ (dashed lines) at $q_s = q_c = -0.005$ C/m^2 (thin lines) or $q_s = q_c = -0.02$ C/m^2 (thick lines). Lines show contours of the relative difference and region below and to the right of each line corresponds to the values of a/r_c and τ at which the relative difference is smaller than the number specified on the line.

for small τ, and lower than the PB-N values at high charge density ($q_s = q_c = -0.02$ C/m^2).

4. Discussion

For the same configuration with the present study, i.e. a charged spherical solute suspended in an electrolyte solution within a charged circular cylindrical pore, there are pioneering works by Smith & Deen (1980, 1983), which presented analytical expressions for the interaction energy E based on the DH equation. By truncating the series expansion for the interaction energy, Deen and his coworkers calculated approximately the solute partitioning coefficient Φ, the hindrance factors H, W as well as the osmotic reflection coefficient (Smith & Deen 1980, Smith & Deen 1983, Deen 1987, Bhalla & Deen 2009, Dechadilok & Deen 2006, Dechadilok & Deen 2009). In a previous study, we adopted the PB equation to estimate the interaction energy and the osmotic reflection coefficient (Akinaga et al. 2008). In a following study, we employed the DH equation to estimate the hindrance factors H and W by a numerical computation Otani et al. (2011), since the linear DH equation is much easier to solve compared to the nonlinear PB equation.

With regard to the difference between the linear DH and nonlinear PB formulations,

Bhalla & Deen (2009) pointed out that the interaction energy $E(\beta)$ can be computed with sufficient accuracy using the DH equation, high charge densities notwithstanding. In contrast, our recent preliminary study suggested that there may be a noticeable difference of the interaction energy in the nonlinear PB and linear DH formulations (Akinaga & Sugihara-Seki 2011). This was the motivation of the present study.

As apparent from figure 4, the present study showed that the ratio of the Boltzmann factors obtained from the PB and DH equations is not always near unity, indicating that the PB and DH Boltzmann factors are not necessarily comparable, especially in the cases of large charge densities and low ion concentrations. This result is in contrast to that of Bhalla & Deen (2009), despite the fact that their parameter ranges are similar to ours. Their comparison of Boltzmann factors obtained from the PB equation and from the DH equation (figure 1 of Bhalla & Deen (2009)) was made only for the solute placed on the pore centerline ($\beta = 0$). This may be one of the causes for the discrepancy between the present result and Bhalla & Deen (2009), since the DH equation gives rather better approximation for the solute on the pore centerline compared to off-axis positions, as shown in figures 3 and 4. Another possible cause may be related to the tendency that the larger the interaction energy is, the smaller the Boltzmann factor is. As representatively shown by open circle and rectangle symbols in figures 3(b) and 4(b), the cases of strong electrostatic interaction with large interaction energy tend to exhibit large relative differences between the PB and DH Boltzmann factors (see figure 4(b)), while the Boltzmann factors themselves are visually indistinguishable in these cases (see figure 3(b)). Thus, the difference between the PB and DH Boltzmann factors may be hardly seen in a linear scale as in figure 3 in the present study or in figure 1 of Bhalla & Deen (2009).

Using the DH equation, O-tani et al. (2011) concluded that even at rather large ion concentrations, the repulsive electrostatic interaction between the solute and pore wall of like charge could significantly reduce both of diffusive and convective transport rates of the solute. Although this conclusion is qualitatively unaltered, the present study suggests that much attention is needed for quantitative estimate of the transport coefficients based on the DH equation, particularly when the charge densities are large or the ion concentration is low or the solute size is large. Figures 5(b), 6(b) and 7(b) indicate that in the case of high charge density ($q_\mathrm{s} = q_\mathrm{c} = -0.02$ C/m^2), the Φ, H, W values obtained from the DH equation are less than a half of those obtained from the PB equation at $\tau \lesssim 4.5$ for $a/r_\mathrm{c} = 0.2$, $\tau \lesssim 6$ for $a/r_\mathrm{c} = 0.4$ and $\tau \lesssim 9$ for $a/r_\mathrm{c} = 0.6$. In the case of low charge density ($q_\mathrm{s} = q_\mathrm{c} = -0.005$ C/m^2), on the other hand, the Φ, H, W values obtained from the DH equation and from the PB equation coincide with each other within 20 % errors at $\tau \gtrsim 4.5$ for $a/r_\mathrm{c} = 0.6$ and $\tau \gtrsim 3$ for $a/r_\mathrm{c} = 0.4$. For $a/r_\mathrm{c} = 0.2$ and $q_\mathrm{s} = q_\mathrm{c} = -0.005$ C/m^2, the differences are within 7 % for all τ values examined in the present study.

In order to delineate the difference more clearly, we plotted in figure 8 the relative difference of the partition coefficient $\Delta\Phi/\Phi_{\mathrm{PB-N}}$ in the parameter space of (a/r_c, τ), where $\Delta\Phi$ represents either $|\Phi_{\mathrm{PB-N}} - \Phi_{\mathrm{DH-A}}|$ or $|\Phi_{\mathrm{PB-N}} - \Phi_{\mathrm{DH-N}}|$ at $q_\mathrm{s} = q_\mathrm{c} = -0.005$

C/m^2 or -0.02 C/m^2. Lines in figure 8 show contours of the relative difference. Since, in general, the relative difference decreases for smaller a/r_c and larger τ at constant charge densities, region below and to the right of each line corresponds to the parameter values at which the relative difference is smaller than the number specified on the line. Thus, displacing a contour line to the left indicates an improvement of the accuracy in this figure. In the case of low charge density ($q_s = q_c = -0.005$ C/m^2), the line of 1 % difference for DH-N is placed on the left-hand side relative to the line for DH-A to a considerable extent, indicating that DH-N provides better results compared to DH-A. In the case of high charge density ($q_s = q_c = -0.02$ C/m^2), on the other hand, the relative difference is generally large for both of DH-N and DH-A. The relative difference is about 10 % along lines running through $(a/r_c, \tau) \sim (0.2, 8)$, $(0.4, 10)$ and $(0.6, 12)$.

It may be interesting to note that the approximate analytical results of Φ, H or W denoted by DH-A sometimes provide better approximation than those of DH-N. This can be explained from the trend that the interaction energy of DH-A is smaller, i.e. the Boltzmann factor is larger, than that of PB-N or DH-N at large β, as shown in figure 3(a), which may compensate the overestimate of the interaction energy of the DH equation.

5. Conclusion

By using an electrostatic model for the solute transport across a membrane with circular cylindrical pores, we examined the effect of the solute and pore charge on the diffusive and convective transport of the solute. The electrostatic repulsive interaction between the solute and the pore was found to reduce the transport rate, especially in the case of large solute size, large charge densities and low ion concentration. The limitation of the DH approximation to the PB formulation was elucidated for the Boltzmann factor and this limitation was shown to be also applicable to the hindrance factors.

Acknowledgments

This research has been supported in part by the Grant-in-Aid for Scientific Research (B) (No. 23360087) from JSPS and the Special Research Fund, Kansai University.

References

Adamson R H, Huxley V H & Curry F E 1988 *Am. J. Physiol.* **254**, H304–H312.
Akinaga T, Sugihara-Seki M & Itano T 2008 *Jpn Phys. Soc. Jpn* **77**, 053401-1–053401-4.
Akinaga T & Sugihara-Seki M 2011 *Journal of Biorheology.* **Submitted**.
Bhalla G & Deen W M 2009 *J. Colloid Interface Sci.* **333**, 363–372.
Curry F E 1984 *Mechanics and thermodynamics of transcapillary exchange* Vol. 4 of *Sec. 2 The Cardiovascular System* Am. Physiol. Soc.
Dechadilok P & Deen W M 2006 *Ind. Eng. Chem. Res.* **45**, 6953–6959.
Dechadilok P & Deen W M 2009 *J. Membrane Science* **336**, 7–16.
Deen W M 1987 *AIChE J.* **33**, 1409–1425.

O-tani H, Akinaga T & Sugihara-Seki M 2011 *Fluid Dynamics Research* **in press**.

Probstein R 2003 *Physicochemical hydrodynamics* A John Wiley & Sons, Inc.

Smith F G I & Deen W M 1980 *J. Colloid Interface Sci.* **78**, 444–465.

Smith F G I & Deen W M 1983 *J. Colloid Interface Sci.* **91**, 571–590.

Smith F G I 1981 Electrostatic effects on the restricted diffusion of macromolecules PhD thesis Massachusetts Institute of Technology.

Sugihara-Seki M 2004 *Fluid Dynamics Research* **34**, 59–76.

Truskey G A, Yuan F & Katz D F 2004 *Transport Phenomena in Biological Systems* Pearson Education, Inc.